

Binary Central Stars of Planetary Nebulae Discovered Through Photometric Variability V: The Central Stars of HaTr 7 and ESO 330-9

Todd C. Hillwig¹

todd.hillwig@valpo.edu

David J. Frew^{2,3}

Nicole Reindl⁴

Hannah Rotter^{1,5}

Andrew Webb¹

Steve Margheim⁶

ABSTRACT

We find the central stars of the planetary nebulae (PNe) HaTr 7 and ESO 330-9 to be close binary systems. Both have orbital periods of less than half a day and contain an irradiated cool companion to the hot central star. We provide light curves, spectra, radial velocity curves, orbital periods, and binary modeling results for both systems. The binary modeling leads to system parameters, or ranges of allowed parameters for each system. We find that for the CS of HaTr 7 we need to use limb-darkening values for the cool companion that are different than the expected values for an isolated star. We also fit the central star spectrum

¹Department of Physics and Astronomy, Valparaiso University, Valparaiso, IN 46383

²Department of Physics, The University of Hong Kong, Pokfulam Road, Hong Kong SAR, China

³Laboratory for Space Research, The University of Hong Kong, Pokfulam Road, Hong Kong SAR, China

⁴Department of Physics and Astronomy, University of Leicester, University Road, Leicester, LE1 7RH, United Kingdom.

⁵Current address: Department of Astronomy, San Diego State University, 5500 Campanile Drive, San Diego, CA 92182, USA

⁶Gemini Observatory, Southern Operations Center, Casilla 603, La Serena, Chile

to determine $\log g$ and temperature values independent of the binary modeling. For ESO 330-9 we find that based on our binary modeling the hot central star is most likely a post-RGB star with a mass of around $0.4 M_{\odot}$. We discuss our derived stellar and nebular parameters in the broader context of close binary central stars and their surrounding PNe. We also discuss the present status of known or suspected post-RGB stars in PNe.

Subject headings: binaries: close — planetary nebulae: individual (PN HaTr 7, ESO 330-9)

1. INTRODUCTION

As the sample of known close binary central stars of planetary nebulae (CSPNe) increases, we are able to begin to compare characteristics of the central stars (CSs) and companions. For example, with the exception of Hen 2-428 (Santander-García et al. 2015), all existing models give CSs that are post-AGB stars consistent with existing stellar evolution models (e.g. Schönberner 1983; Bloeker 1995). However, there is some evidence that a handful of PNe may have post-RGB CSs (see §4 for further discussion). We also find that cool companions in close binary CSPNe are typically over-luminous compared to their main sequence (MS) counterparts, presumably due to the irradiation effect from the hot nearby CS. To date, no brown dwarf or planetary companions have been found in close orbits with CSPNe, though an increasing percentage of double degenerate (DD) systems are being discovered and it is possible that there are as many close binary CSPNe with white dwarf (WD) companions as those with MS companions (c.f. Hillwig 2014).

We can also compare resulting binary system parameters such as orbital period distribution and orbital inclination relative to the surrounding planetary nebula (PN). The orbital period distribution of known close binary CSPNe is similar to systems without a PN (either because the ejected envelope was never visible or because the system is past the PN stage), though it is possible that the CSPNe systems have a slightly longer period distribution (Hillwig 2011). Both distributions show very few systems with periods greater than a few days, suggesting that the common envelope (CE) phase is very efficient in reducing the orbital separation of the two stars. This is consistent with recent work on CE evolution (e.g. Ricker & Taam 2012; Passy et al. 2012; Nandez et al. 2015; Iaconi et al. 2016; Ohlmann et al. 2016). Though broad examination of possible initial binary parameters has not been performed due to complexities of the CE evolution process and limitations on computational abilities, significant headway is being made on our understanding of the CE process. With further work in both CE simulations and observational determination of stel-

lar and orbital parameters of close binary CSPNe, more detailed and statistically significant comparisons will be possible.

Hillwig et al. (2016b) have shown a clear link between the inclinations of close binary CSPNe and their associated PNe, demonstrating a physical connection between the two. Such a connection has long been suspected (and expected in some cases) with a number of papers showing correlations between, e.g. strongly bipolar PNe and post-CE CSs (Zijlstra 2007; De Marco 2009; Miszalski et al. 2009).

Apart from studies of the stars themselves, work is being done on relating the nebula around close binary CSPNe. Corradi et al. (2015) show a relationship between close binary CSPNe and abundance discrepancies in their associated PNe (see also Jones et al. 2016). Considering the abundance discrepancies and low ionized mass of many of these PNe (also discussed by, e.g. Frew 2008; Frew & Parker 2007) they suggest the possibility that these may not be PNe at all, but some later stage of mass loss or even the disruption of a Jupiter-mass planet.

One goal of this series of papers (De Marco, Hillwig, & Smith 2008) has been to use photometric monitoring to discover additional close binary CSPNe to improve the binary parameter statistics. Here we present two newly discovered systems: the CSs of HaTr 7 and ESO 330-9. Both are irradiated binary systems with cool companions and have orbital periods of less than half a day. Below we show multi-color photometry, spectra, and radial velocity curves for both systems and calculate parameter sets for both using the Wilson-Devinney binary modeling code (Wilson & Devinney 1971; Wilson 1990).

2. The Central Star of the Planetary Nebula HaTr 7

2.1. Background

The faint PN Hartl-Tritton 7 (HaTr 7, PN G332.5-16.9) was discovered on UK Schmidt plates by Hartl & Tritton (1985). They describe the nebula itself as a “slightly elliptical disk with very low surface brightness”.

Saurer et al. (1997) provide a spectrum of the CS of HaTr 7 showing both absorption from the CS and emission lines near 4650 Å. This type of emission in CSPNe has often lead to a “weak emission line star” (wells) classification. More recently it has become understood that the wels classification is not a separate physical effect (e.g., Weidmann et al. 2015), but a combination of unrelated causes such as irradiation effects (e.g., Miszalski et al. 2011), residuals from nebular subtraction (e.g., Basurah et al. 2016), and other effects. Saurer et al.

(1997) suggest these lines may be due to carbon enrichment, but we show below that they are irradiation lines from the heated hemisphere of a cool companion. They use a non-LTE model atmosphere including H and He to determine a temperature for the CS of $T_{CS} = 100,000$ K, a surface gravity $\log g = 6.0$, and a CS mass of $M_{CS} = 0.56 M_{\odot}$.

We provide a color composite image of the nebula in Figure 1. The images were obtained with the SOAR 4-meter telescope. Red is from an $H\alpha$ image, green from an O III image, and blue from a B filter image. The dark stripe in the center of the image is from the inter-chip gap on the CCD. While the nebulosity is faint, the general shape looks similar to that of Abell 65 (Hillwig et al. 2015) which Huckvale et al. (2013) found to be a double-lobed PN at an angle of about 62° . It is possible that HaTr 7 has a similar shape and is also at an intermediate angle.

Chu et al. (2009) provide a *Spitzer* MIPS 24 μm band image of HaTr 7. Their image looks very similar to our visible image though with a more pronounced southern “lobe” and a smaller spatial extent. They do not find a point-source at the location of the CS, suggesting that it does not have a strong dust component to its spectrum.

Frew et al. (2016) give a distance to HaTr 7 of 1.85 ± 0.53 kpc and an interstellar reddening value of $E(B - V) = 0.08 \pm 0.03$.

Below we explore in more detail potential binary models and compare our results to the information discussed above.

2.2. Observations and Reductions

The photometric data consist of B , V , and R images obtained with the SARA-CTIO 0.6 meter telescope in 2014 April, 2014 May, and 2015 June. We also utilize 82 V data points from the Catalina Sky Survey (CSS, Drake et al. 2009).

All images were bias subtracted and flat fielded. The IRAF/DAOPHOT¹ package was used to perform aperture photometry on the images. Single star differential photometry was performed on the resulting data with two additional stars used to check the photometric stability of the comparison star. We find that the comparison star is constant with standard deviations from the mean of 0.003 mag in B , 0.005 mag in V , and 0.004 mag in R .

¹IRAF is distributed by the National Optical Astronomy Observatory, which is operated by the Association of Universities for Research in Astronomy (AURA) under a cooperative agreement with the National Science Foundation.

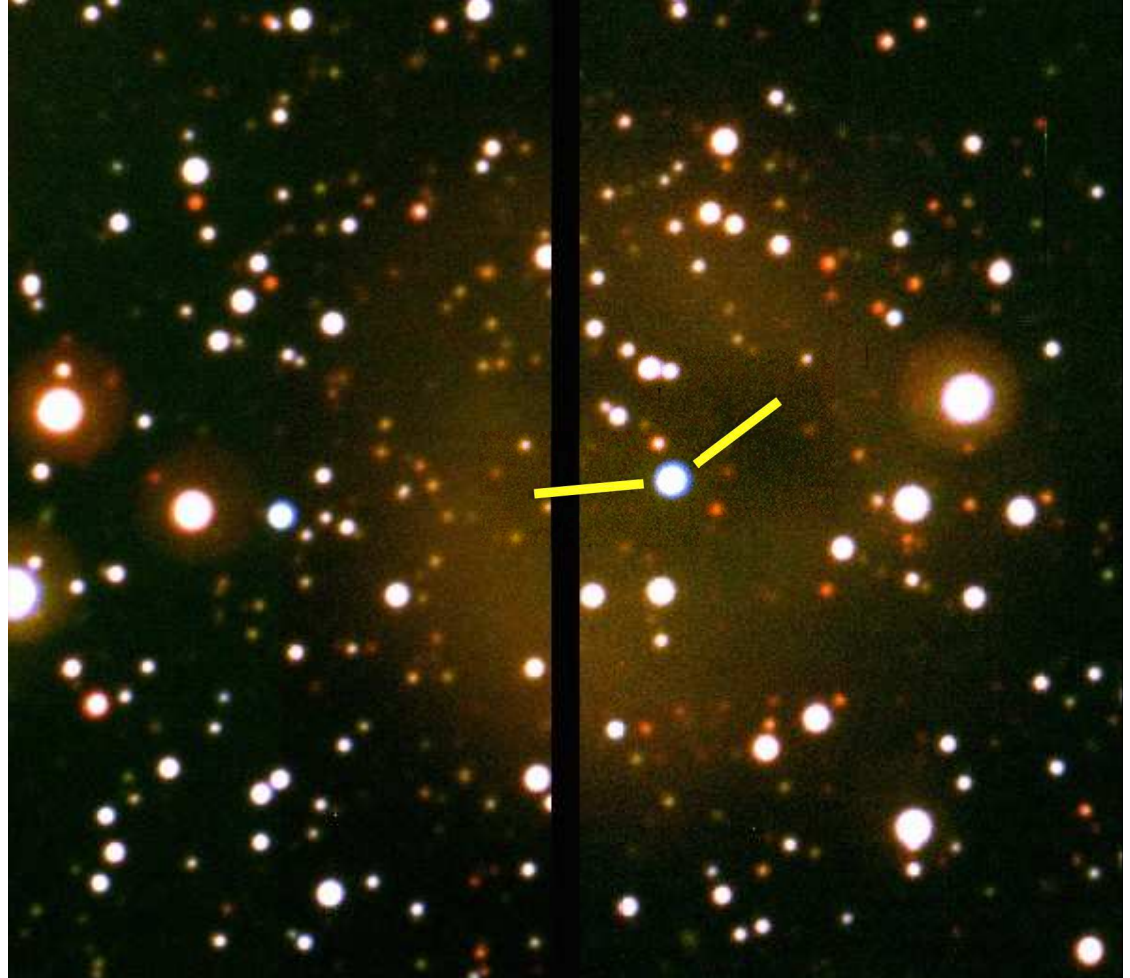


Fig. 1.— A color composite image of HaTr 7 from the SOAR telescope. The CS is the bright blue star at the geometric center of the PN identified by hash marks in the image. North is up and East is to the left.

Using the long baseline of our photometric data and the CSS data together gives a photometric ephemeris of

$$T = 2457203.970(5) + 0.3221246(8) \times E \text{ days.}$$

Here E is the number of orbits since time T_0 , with $E = 0$ corresponding to minimum light measured in heliocentric Julian date. In Figure 2 we show the CSS V data along with our V data, where we have shifted our data to the apparent magnitude scale of the CSS data. Figure 3 shows the B , V , and R light curves for HaTr 7 along with an example binary model (described further below). We do not include the CSS V data in this plot because of the larger scatter and uncertainties and for visibility of the model lines compared to the data.

We also obtained orbit-resolved spectra in 2016 June using GMOS on the Gemini-South telescope in longslit mode with the B1200 grating and a $0.75''$ wide slit. The spectra cover a range of $3825\text{--}5442 \text{ \AA}$ with a resolution of $R = 3744$ and 2×2 binning resulting in 0.516 \AA per pixel. The IRAF/Gemini package was used to reduce the spectra. Wavelength calibration used CuAr arc spectra taken consecutively with the science spectra, giving a typical radial velocity calibration of approximately 0.2 \AA or better.

A spectrum near maximum light (Figure 4a) shows strong emission lines consistent with an irradiated companion. In addition, there are N V $\lambda\lambda$ 4604, 4620 \AA , He II, and hydrogen Balmer absorption lines from the hot CS. The spectrum in Figure 4b obtained close to minimum light shows a near absence of emission lines, suggesting an irradiated binary at a moderate to high inclination such that the hottest portion of the cool star, the sub-stellar point nearest the hot CS, moves out of view for that portion of the orbit. The minimum light spectrum also provides an opportunity to reassess the model atmosphere of Saurer et al. (1997). Given the strong emission lines near 4650 \AA in their published spectrum, it must have been obtained near maximum light. For our observed photometric amplitude, at that orbital phase the heated secondary is contributing as much as 30% of the system light. Thus the absorption lines will be weakened by the additional light source. If we assume that the light from the secondary is negligible at minimum light, the line depths are then representative of the CS alone.

For the quantitative spectral analysis we used the model grid from Reindl et al. (2016), which was calculated with the Tübingen non-LTE model-atmosphere package (TMAP², Werner et al. 2003; Rauch & Deetjen 2003). The parameter fit was performed by means of a χ^2 minimization technique with SPAS (Spectrum Plotting and Analysing Suite, Hirsch 2009), which is based on the FITSB2 routine (Napiwotzki 1999). We fitted all Balmer and

²<http://astro.uni-tuebingen.de/TMAP>

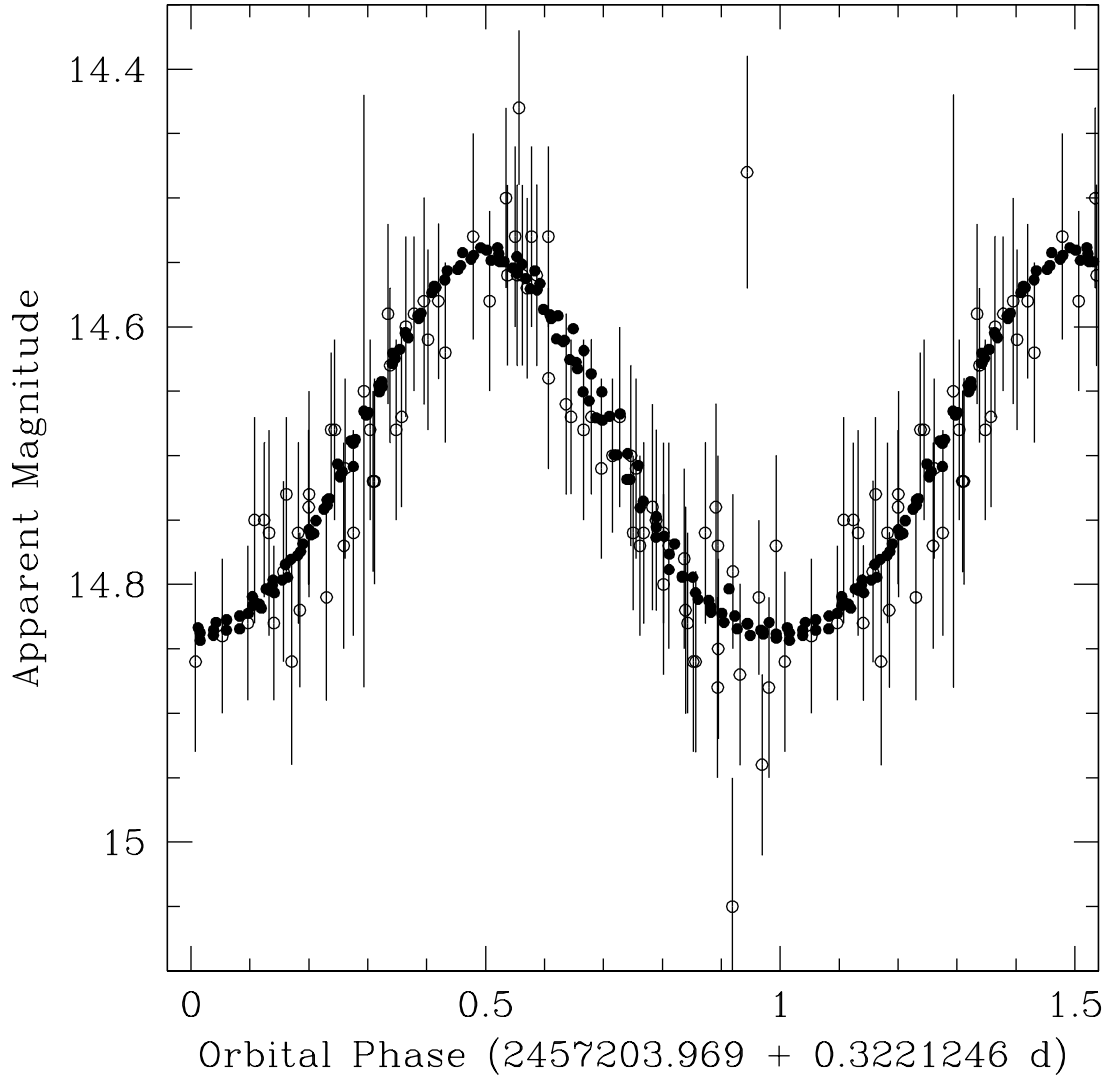


Fig. 2.— The V -band photometry from CSS (*open circles*) and SARA-CTIO (*filled circles*) phase-folded onto the ephemeris in the text. The SARA-CTIO data has been shifted in magnitude to match the CSS apparent magnitude scale.

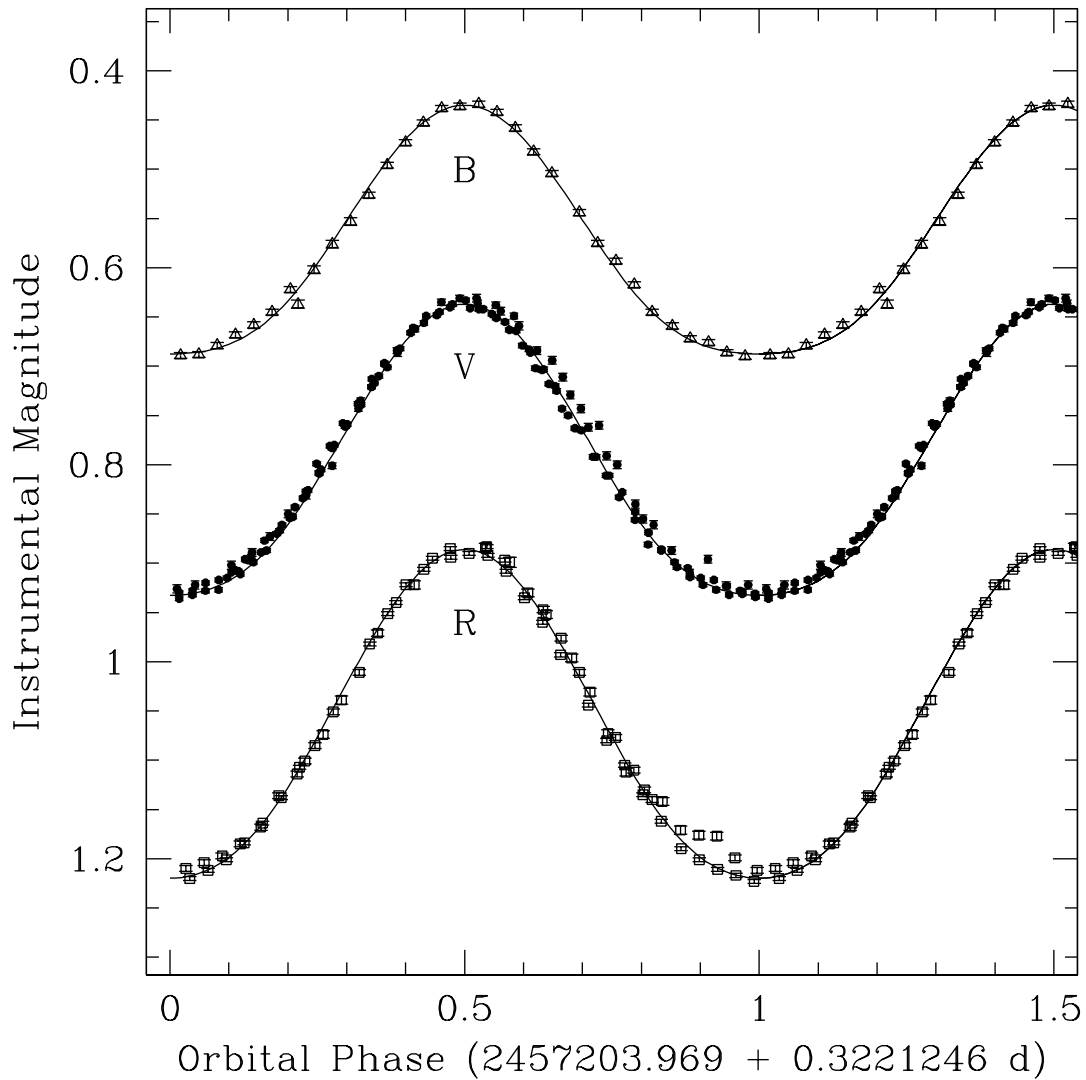


Fig. 3.— The differential magnitude B , V , and R phase-folded light curves of HaTr 7 for the ephemeris in the text. The solid lines correspond to a binary model from the Wilson-Devinney code as described in the text. Error bars are included though in most cases they are smaller than the symbols.

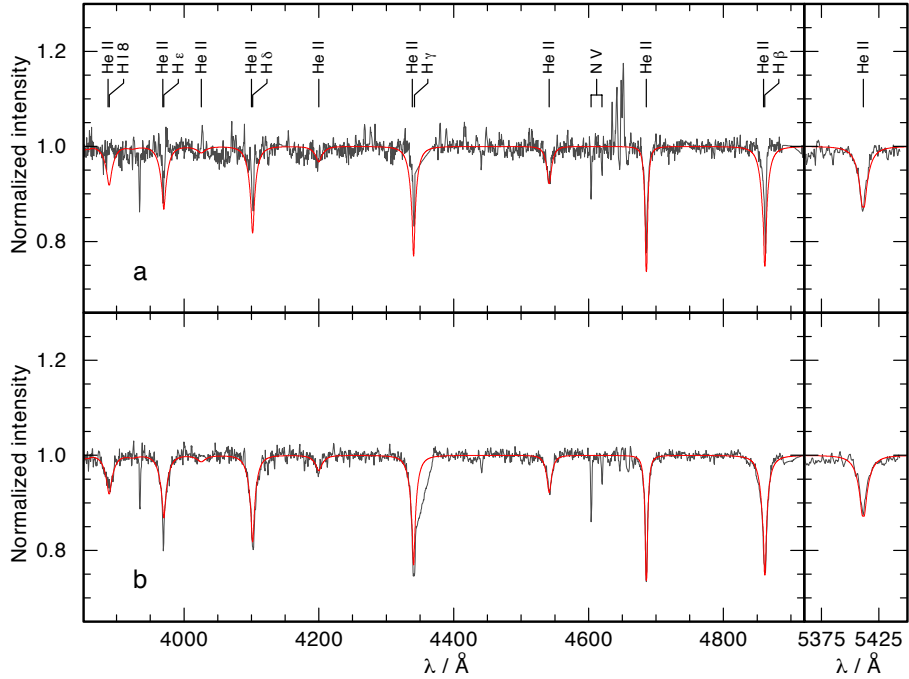


Fig. 4.— Two sample spectra of the CS of HaTr 7 taken near maximum light (a) and minimum light (b). Easily visible is the CNO complex of emission lines near 4650 \AA due to irradiation of a cool companion. Absorption lines from the hot CS are also present and dominate the spectrum in (b). We also show our TMAW model fits giving with $T = 95300 \pm 2000 \text{ K}$ and $\log g = 5.79 \pm 0.04$ in red. Chip gaps near the $H\gamma$ and $H\beta$ absorption features made continuum fitting near these lines difficult in the red wings of the lines.

He II lines detected in the spectrum of HaTr 7. Because of chip gaps overlapping the red wing of H γ and falling very near the red wing of H β , we fit only the blue-ward half of those two lines. Our results give $T = 95300 \pm 2000$ K, $\log g = 5.79 \pm 0.04$, and a log Helium mass fraction $X_{He} = -0.56 \pm 0.03$, close to the solar value. These are in good agreement with Saurer et al. (1997). In Figure 4 we compare our best fit model with the observations. Comparing the TMAP model with the spectrum taken at maximum light (4a), the impact of the light of the companion becomes obvious. While the pure He II line profiles are hardly affected, the the Balmer lines become much more narrow and their intensity is reduced by about 15%.

To derive the mass and luminosity of the stars, we compared the position of HaTr 7 in the $T_{eff} - \log g$ plane with latest H-burning post AGB tracks of Miller Bertolami (2016) (Figure 5). We find that the central star should have a mass of $0.52 M_{\odot}$ and $L = 2000 L_{\odot}$, i.e. $\log(L/L_{\odot}) = 3.3$.

To determine radial velocities for the CS and companion we fit Gaussian profiles to the narrow emission lines and Voigt profiles to the broad absorption features. The C, O, and N emission lines near 4650 \AA are the only strong irradiation lines in the spectrum, so we used the average velocities for those lines to determine a radial velocity for the companion for each spectrum. For the CS we used the average velocity of the visible absorption lines of H I, He II, and N V. The resulting radial velocity curve (Figure 6) confirms that the photometric period is equal to the orbital period. We also see that the emission lines do originate from the companion star, confirming their origin in an irradiated hemisphere of a cool companion.

Sine curve fitting to the CS and companion curves result in velocity zero-points that are different by about 11 km s^{-1} . We address this issue in our binary modeling section below.

2.3. Binarity and System Parameters

For our binary modeling we adopt initial values for the CS mass, $\log g$, and temperature values in the range of our spectral fitting and that of Saurer et al. (1997). The primary difference comes in the CS mass as described above. So we use $0.52 \leq M_{CS} \leq 0.56 M_{\odot}$, $5.5 \leq \log g \leq 0.60$, and $90,000 \leq T_{CS} \leq 100,000$ K. The double-lined radial velocity curve allows us to determine a mass ratio, however we need to be careful about simply using the ratio of the amplitudes of the two curves. Because the companion radial velocity curve is determined using emission lines due to irradiation, the amplitude traces the velocities of the irradiated hemisphere and not the stellar center-of-mass. The amplitude then depends on the radius of the secondary relative to the star’s distance to the system center-of-mass.

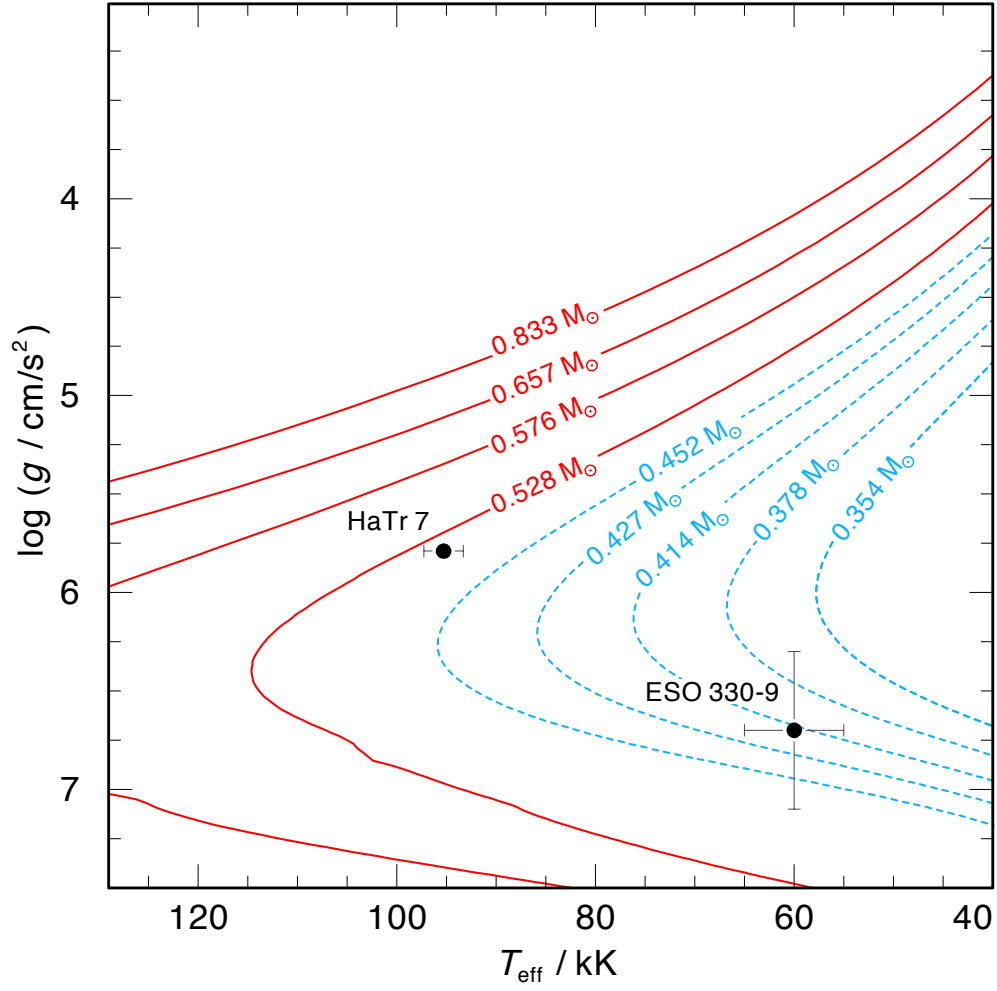


Fig. 5.— Our model results of $\log g$ and T for the CSs of HaTr 7 and ESO 330-9 plotted with the post-AGB evolutionary tracks of Miller Bertolami (2016) (*red solid lines*) and post-RGB tracks of Hall et al. (2013) (*blue dashed lines*).

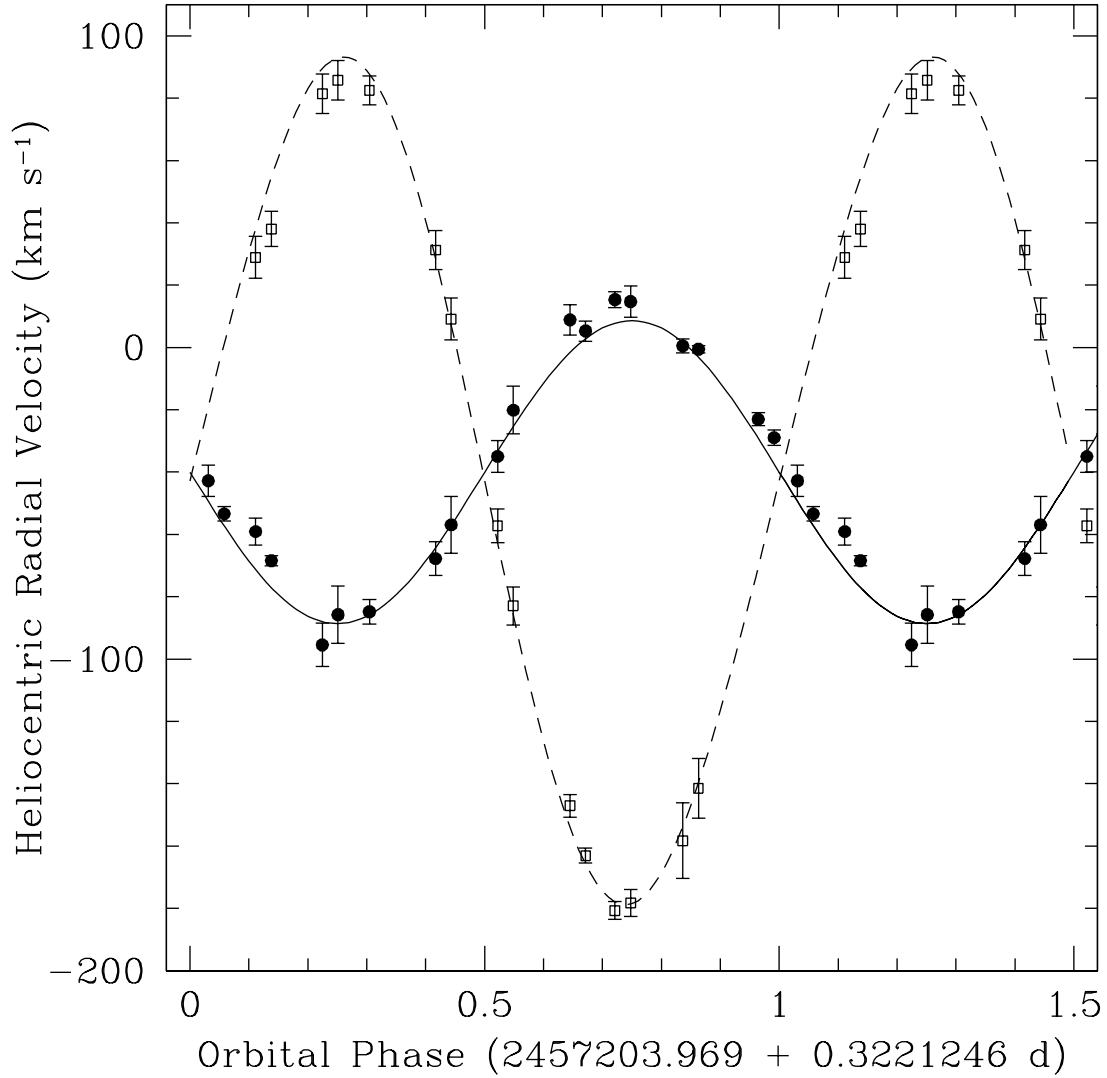


Fig. 6.— The radial velocity curve for the CS of HaTr 7. Data points are for the irradiation lines (*hollow squares*) and absorption lines (*solid circles*) described in the text. The dashed line is the radial velocity curve for the irradiated companion, the solid line is for the CS, based on our Wilson-Devinney modeling.

Therefore, rather than adopting a center-of-mass velocity, we require that the resulting model produce a good fit to the radial velocity data. The ratio of the two amplitudes from sine curve fitting is 0.38, which we use as a maximum expected value for the mass ratio, $q = M_2/M_{CS}$ (assuming that the center-of-mass amplitude of the companion is larger than that found from the emission lines).

As mentioned above, we find that fitting independent sine curves to the two radial velocity curves produces a zero-point offset of about 11 km s^{-1} with the CS at a more redshifted velocity than the companion. Some of this will be due to gravitational reddening from the CS, which in turn depends on the mass and radius of the CS. However, using the mass and $\log g$ values from Saurer et al. (1997) and our modeled values gives a resulting gravitational redshift in the range $2\text{--}3 \text{ km s}^{-1}$, which only corrects about one-quarter of the observed shift. The cause of the remaining shift is unclear. Zero-point offsets in the spectra should produce identical behavior in the CS and companion, rather than opposite shifts. It is possible that the emission lines from the companion are being created high in the atmosphere and that a wind could produce an additional blue-shift. These are speculation however and without knowing if it is an intrinsic or data cause, we correct for the CS gravitational redshift and proceed with the binary modeling to achieve the best possible fit to the existing data.

The first result we find from our binary modeling is that for the temperature of the CS and relative sizes of the CS and companion, the temperature of the companion is not well constrained. Any temperature below about 5000 K produces almost identical light curve amplitudes. We believe that this effect is essentially due to a “saturation” of the irradiation effect in the atmosphere of the companion. That maximum temperature does change slightly depending on the rest of the system parameters, but we find that a companion temperature of 4500 K is indistinguishable from lower temperatures for all of our remaining parameter sets. Thus for all of our models we set the companion temperature at 4500 K.

From Figure 3 we see that the light curve amplitudes in B , V , and R are measurably different, with the R amplitude being the largest and B the smallest. For these types of binaries, this trend in amplitudes usually means that the companion provides a significant contribution to the total light of the system even disregarding the irradiation effect. However, the small orbital period and small mass ratio give a correspondingly small orbital separation and Roche lobe radius for the companion, meaning that the maximum volume radius for the companion should be less than $0.5 R_{\odot}$. In this case, the companion would *not* contribute significant light to the system.

Proceeding with our binary modeling we indeed find that for realistic companion stars we cannot reproduce the relative light curve amplitudes by adjusting only the inclination and stellar masses, radii, and temperatures. We find that for realistic stellar parameters, when

the binary model light curves fit the observed B amplitude, the V and R amplitudes are too small (the R being more discrepant than the V). And vice versa, when we match the model curves to the R filter, the V and B model curves have amplitudes larger than the data. Only for CS temperatures *much* lower than those consistent with the CS spectrum and its lack of He I lines (requiring $T_{CS} > 70,000$ K) do we find matches for the relative amplitudes. The only means of producing a parameter set that matched the data was to use limb darkening coefficients different than those calculated internally by the Wilson-Devinney code. While there have been close binary CSPNe for which different limb-darkening coefficients have been reported, even limb-brightening (e.g., Bond & Grauer 1987; Pollacco & Bell 1994), as a default we use the internally calculated values unless, in situations like this, it is clear that those values will not provide a match to the data. The difficulty with changing limb darkening coefficients is that at this point those changes are purely empirical. Without a better understanding of the physical changes in limb darkening any changes are essentially arbitrary and can produce very large changes in the resulting light curve amplitudes. We choose to modify limb-darkening values rather than another stellar parameter or parameters such as albedo or gravity darkening because, as described above, previous studies have suggested that limb-darkening of the cool companions in these systems may be different than the expected values for their MS equivalents. And it is easy to understand physically how limb-darkening could be different for an irradiated atmosphere in which, if the effect is large enough, a temperature inversion may take place in the stellar photosphere.

We initially used a quadratic form for the limb darkening, but find that a linear form produces nearly identical results and provides a better intuitive understanding of the required changes. Here we use the linear form $I(\mu)/I(1) = 1 - u(1 - \mu)$ from Claret (2000) where $I(1)$ is the intensity at the center of the stellar disk, $\mu = \cos \gamma$, and γ is the angle from the line of sight from the stellar center to the point of emission on the stellar surface. Thus smaller values of u result in a less limb darkened disk, values of $u > 1$ are not physical, and values of $u < 0$ would result in limb brightening. In this case, we find that the more red filters require larger negative changes in limb darkening than the bluer filters. Thus for example, if we leave the B filter limb darkening at the expected value for the companion star, the V and R limb darkening values must be reduced, such that the V limb darkening is somewhat reduced from its expected value and the R limb darkening is significantly below its expected value. In other words, the redder the wavelength, the less the star is limb-darkened. Using the linear limb-darkening coefficients from Claret (2000) we find values for the companion of $u_B = 0.881$, $u_V = 0.796$, and $u_R = 0.723$ for a temperature of 4500 K and $\log g = 4.5$. In order to fit the data, keeping u_B constant, we find values of $u_V = 0.610$ and $u_R = 0.152$. Allowing u_B to change as well results in different modeled radii for the companion. Reducing the limb darkening further results in smaller radii, while increasing u_B results in larger radii.

The radius changes by less than 10% in each direction unless the limb-darkening values become negative as they decrease, or unphysical as they increase.

We provide in Table 1 a range of system parameters which provide acceptable fits to the data. We find that the CS agrees with evolutionary models of post-AGB stars, as expected based on using values consistent with model spectra. Our modeled parameter range also includes our spectroscopically determined values for the CS in temperature, radius, $\log g$, and luminosity. In Figure 5 we plot the CS in $\log g$ vs temperature along with post-AGB models of Miller Bertolami (2016) and post-RGB models of Hall et al. (2013). Each of the parameter combinations we found results in a companion star larger than we would expect for a MS star of its mass. Given our inability to determine a precise temperature for the secondary, we cannot speak directly to how its temperature would compare to that of a similar MS star. However, the upper limit to the temperature is higher than equivalent MS temperatures for all ranges of our companion star parameters. So our companion temperature is consistent with or slightly higher than for an equivalent MS star. Over-luminous companions due to larger radii and/or higher temperatures are typical in the cool companions of close binary CSPNe.

The inclination of the binary system we find to be $i = 45 - 50^\circ$. While we do not have an inclination for the PN, our visual inspection described above did suggest an intermediate inclination. Thus our binary inclination is at least consistent with that expectation.

Using the $E(B - V)$ value from Frew et al. (2016) and a measured apparent magnitude we can use our model to calculate a distance to HaTr 7. The available apparent visual magnitudes are consistent within our observed 0.3 magnitude amplitude variability in the light curve. The SPM 4 catalog (Girard et al. 2011) gives an estimated $V = 15.03$, the UCAC 4 catalog (Zacharias et al. 2012) gives $V = 15.111$, and the APASS value is $V = 14.954 \pm 0.232$ (Henden et al. 2016). However, we do not know at what phase these data were obtained. Using the data from the Catalina Sky Survey, we find a minimum-light value of $V = 14.84 \pm 0.08$ where the error is based on both the scatter in the light curve and the zero-point calibration of the CSS data. While this minimum value is slightly brighter than the SPM 4, UCAC 4, and APASS values, they are consistent given the uncertainties of those measurements. Using the minimum-light value from the CSS data of $V = 14.84$ and using $E(B - V) = 0.08$, we find a de-reddened apparent visual magnitude of the CS of HaTr 7 of $V = 14.57 \pm 0.08$. From our binary model we find a total system brightness at minimum light of $2.5 < M_V < 3.2$. From these values we calculate a distance range from our model of $1.9 < d < 2.6$ kpc, which agrees well with the distance of 1.85 ± 0.53 kpc from Frew et al. (2016). Frew et al. (2016) also used the atmospheric parameters from Saurer et al. (1997) to determine a spectroscopic “gravity??” distance of 1.80 ± 0.70 kpc (see their Table 5).

Using our revised parameters for the ionizing star, a nearly identical distance of 1.90 ± 0.50 kpc is calculated, our lower gravity estimate essentially canceling out the brighter V -band magnitude we now use. This value is also in very good agreement with the surface brightness distance.

3. The Central Star of the Planetary Nebula ESO 330-9

3.1. Background

ESO 330-9 (PHR J1602-4127; PN G331.0+08.4) was first noted on the ESO Sky Survey (Lauberts 1982), and described as either an emission nebula or galaxy. It was re-discovered and identified as a planetary nebula in the MASH Survey by Parker et al. (2006), though Magakian (2003) catalogued it as a reflection nebula (GN 15.58.9). MASH spectroscopy reveals the nebula to have a relatively modest excitation (see Frew 2008) and narrowband images are additionally presented by Boffin et al. (2012). ESO 330-9 is currently classified as a likely PN by Parker et al. (2016). Frew (2008) also gave a distance of 1.65 kpc and noted that based on available data the CS appeared to have an IR excess and was thus a good candidate for having a cool companion. Very little further work has been done on the PN or central star. Figure 7 shows a color image of the nebula from the POPIPLAN survey (Boffin et al. 2012) using [O III] and $H\alpha$ +[N II] images from the VLT. The CS, which was identified by MASH is off-center relative to $H\alpha$ +[N II] (purple in the image), but is relatively well-centered in O III (green). The abrupt and brightened south-eastern edge suggests interaction with the ISM, which may be the cause of the asymmetry. A dark lane is also visible near the edge of the central [O III] emission.

Frew et al. (2016) give a mean distance of 1.73 ± 0.51 kpc to ESO 330-9 and an $E(B - V) = 0.27 \pm 0.10$. However, the line-of-sight reddening from Schlafly & Finkbeiner (2011) is $E(B - V) = 0.64$. We explore this further below.

The reported visual apparent magnitude of the CS from the SPM 4 catalog (Girard et al. 2011) is $V = 16.86 \pm 0.2$. However, the YB6 catalog³ gives $V = 15.76 \pm 0.4$ so it is difficult to determine from these a precise value for the visual magnitude. DENIS and 2MASS give more reliable values for the near-IR magnitudes $I = 16.04 \pm 0.06$ (DENIS), $J = 15.07 \pm 0.14$ (DENIS), $J = 15.36 \pm 0.05$ (2MASS), $H = 14.54 \pm 0.07$ (2MASS), and $K_s = 14.38 \pm 0.07$

³YB6 = Yello-Blue all-sky catalog, version 6: Monet, D.G. 2004, complete scan of USNO NPM and SPM plates

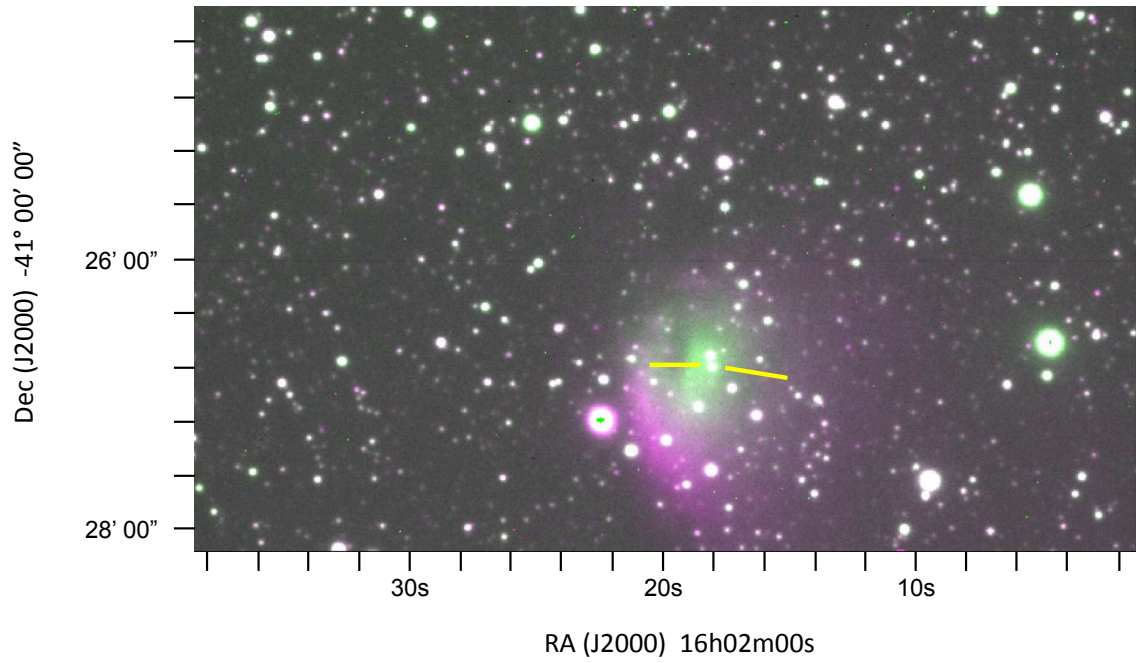


Fig. 7.— A tricolor RGB image of ESO 330-9 from the POPIPLAN survey [O III] (*green*) and $H\alpha+[N II]$ (*red and blue*) images. The CS is identified by hash marks in the image.

(2MASS). The difference in the DENIS and 2MASS J magnitudes is not due to intrinsic variability, as the orbital phase of the two measurements are only different by about 0.08. The dates at which the measurements were obtained are too far separated in epoch from our data to allow proper determination of the actual orbital phase, but even for phases providing the maximum magnitude difference we find from our models over a 0.08 orbital phase difference $\Delta J = 0.06$. At that level the two values marginally agree with one another. We also find a GALEX measurement of the near-UV giving $m_{NUV} = 17.97 \pm 0.045$.

There is no age determination for the PN. Part of the difficulty in an age determination is the apparent ISM interaction, which makes determining an age based on the size and expansion rate of the nebula very difficult. There is also no published value for the expansion rate of the nebula. But the nebular size reported by Frew et al. (2016) of $200''$ by $175''$ gives an average radius of about $95''$. If we then assume a typical expansion speed of about 10 km s^{-1} , we find a very approximate age of 78,000 years for the distance of 1.73 kpc.

3.2. Observations and Reductions

Our photometric data were obtained with the 0.6m SARA-CTIO telescope in 2013 April, May, and June in the V filter and 2013 June and July in the B and R filters. The images were bias subtracted and flat fielded. The IRAF/DAOPHOT package was used to perform aperture photometry on the images then single-star differential photometry was used to obtain a light curve. Two additional check stars were used to verify the stability of the comparison star, which was constant to 0.015 mag in both B and V and to 0.008 mag in R . We find an orbital ephemeris (assuming a binary system) of

$$T = 2455294.6925(5) + 0.29592(4) \times E \text{ days.}$$

where $E = 0$ occurs at minimum light.

Figure 8 shows our V -band light curve folded on the ephemeris above. Our first set of observations at minimum light are significantly fainter than the remaining observations at minimum light. We initially thought that the system may show ellipsoidal variability with two different minima. But later photometry and radial velocity data confirmed the irradiation effect and shorter orbital period (equal to the photometric period rather than twice the photometric period). We explored data processing sources for the fainter magnitudes in that portion of the one night of data, but ruled out throughput, seeing, or comparison star causes. At this point we assume that the cause is intrinsic to the system, perhaps an orbiting dust cloud as seen in Grothues & Kohoutek (1993) and Hajduk et al. (2008), though the timescale for the variability in those systems is much longer. In this case the dust would

have to be on a much smaller orbit, or the dust is being produced in a wind and is not following a closed orbit.

In Figure 9 we show three nights of V -band data for ESO 330-9 with our binary model light curve (described below) subtracted from the data. The result shows the variability of the system relative to our binary model. The width of each window is twice the orbital period. We only see the large dimming episode on one night, though the third night does show a small deviation above the uncertainties. The shift brightward in the third night may be intrinsic, though the differential photometry zero point is likely only good to within about 0.01 magnitudes based on night-to-night variations, so we do not take the offset to be significant. No significant dimming (or brightening) episodes are seen in the B or R data. In looking at the episode, the much faster rise time as opposed to the slower decline suggests that the cause is not a transiting planet or some other solid body, but is more likely a dust cloud, if the cause is indeed intrinsic to the system.

Because we cannot find a direct relationship between the dimming episode in our V -band data and the central binary, for our binary modeling we have removed that portion of the data so that we can concentrate on fitting the binary system parameters. In Figure 10 we show the resulting three-filter light curves for ESO 330-9 along with an example model fit. The curves have been shifted vertically for clarity and do not represent relative brightness in the respective filters. As with HaTr 7, we see a marked increase in variability amplitude moving from B to V and R .

A total of 16 spectra of the CS of ESO 330-9 were obtained with the GMOS instrument at Gemini South in long-slit mode with the B1200 grating with a resolution of $R = 3744$. The observations were made in 2013 August with the B1200 grating and a $0.75''$ wide slit. The spectra cover a range of 4010-5475 Å with a spectral resolution of 0.471 Å per pixel. The IRAF/Gemini package was used to reduce the spectra. Wavelength calibration used CuAr arc spectra taken consecutively with the science spectra, giving a typical radial velocity calibration of approximately 0.2 Å or better.

The sample spectrum in Figure 11 shows emission lines from what appears to be an irradiated atmosphere, including the well-recognized C, N, and O complex near 4650 Å, Balmer emission, He I lines at $\lambda\lambda$ 4026, 4388, 4471, and 5015 Å, Mg II λ 4481 Å (partially overlapped by a chip gap), and C II λ 4267 Å. The appearance of the He I emission but no He II suggests a relatively cool CS. However, the faint and relatively broad He II absorption from the CS also helps to confirm the identity of this object as the CS, even though it appears off-center in the visible nebulosity (though it is positioned within the high-excitation [O III] emission).

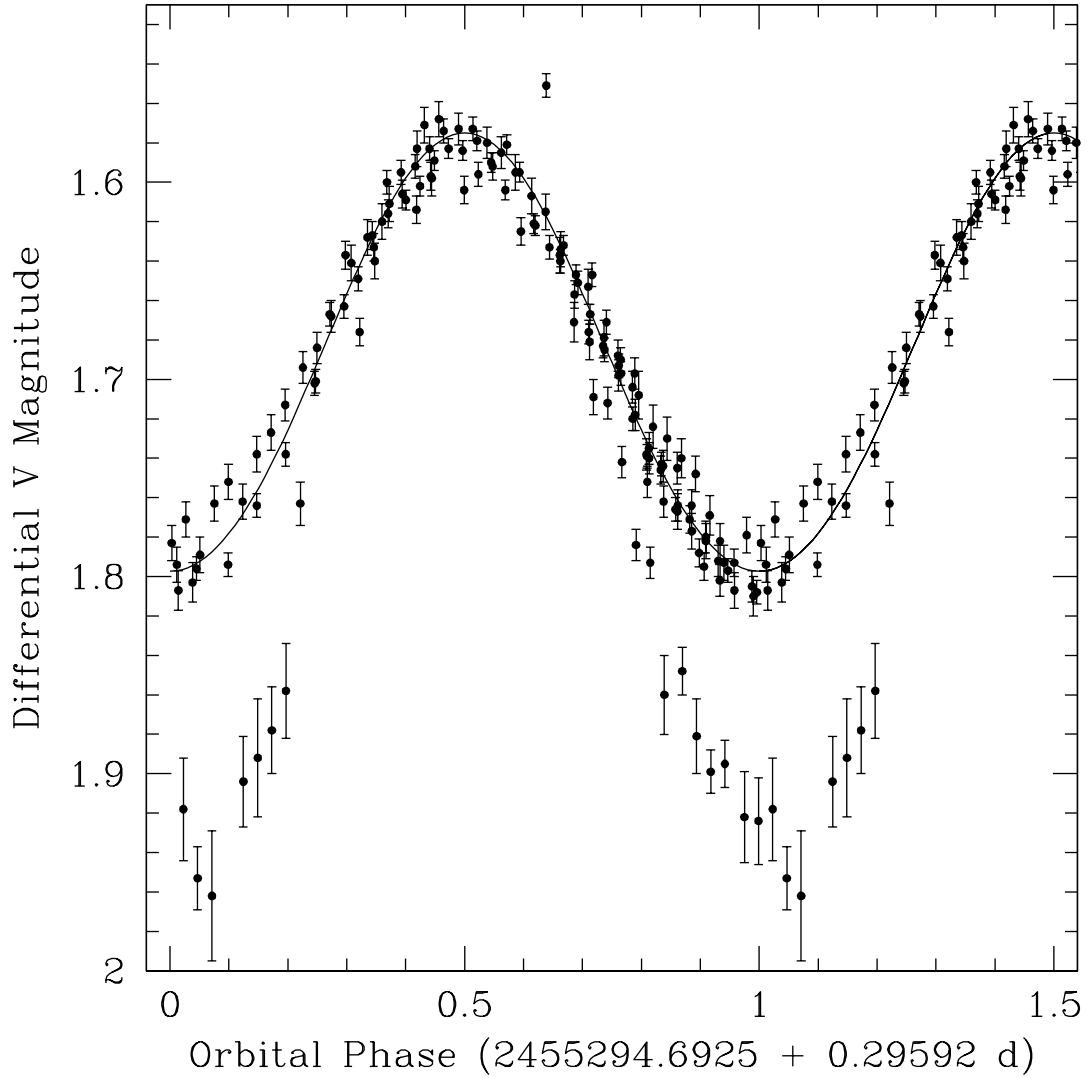


Fig. 8.— Phased differential V magnitude light curve of ESO 330-9 for the ephemeris in the text. The one-time observed decrease in brightness is apparent near minimum light. The line is from the Wilson-Devinney model fit as described in the text.

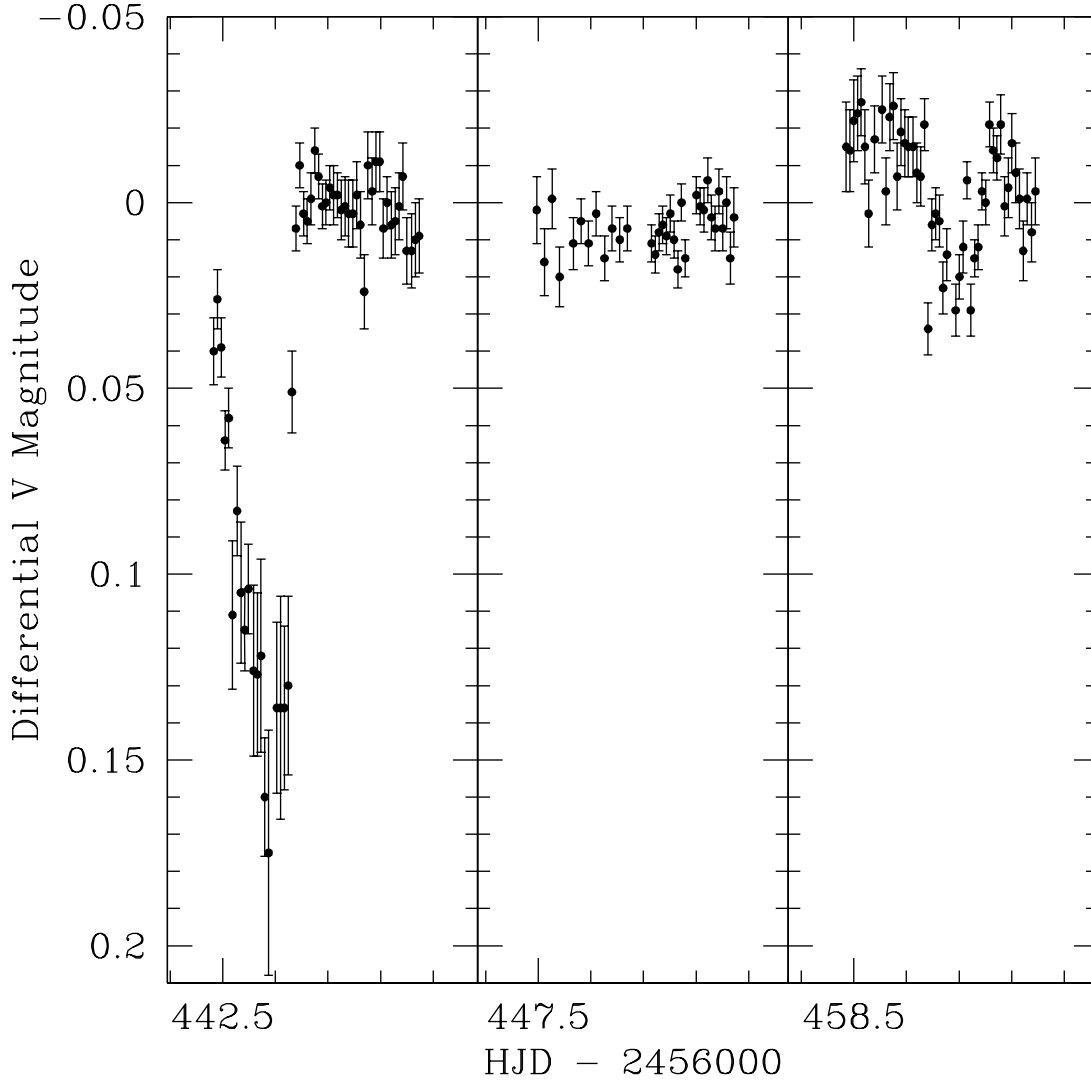


Fig. 9.— Three nights of V -band data with our binary model curve subtracted to show variability other than due to the close binary. The small tick-marks on the x-axis denote steps of 0.1 day.

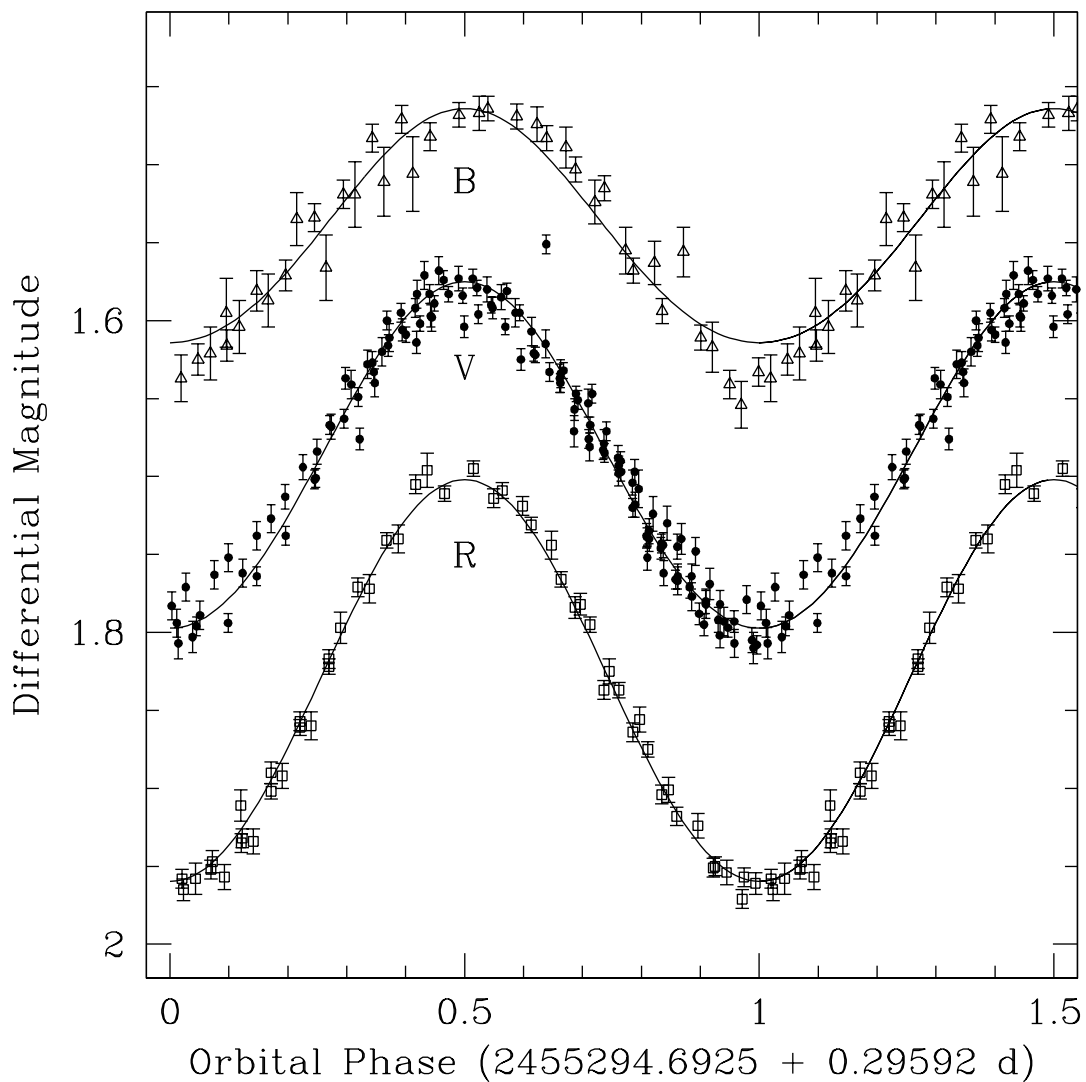


Fig. 10.— Phased differential magnitude B (*triangles*), V (*circles*), and R (*squares*) light curves of ESO 330-9 for the ephemeris in the text. Lines are from Wilson-Devinney model fits as described in the text.

Table 1. HaTr 7 Binary System Parameter Ranges

Parameter	Value
q	0.30 – 0.35
M_{CS} (M_{\odot})	0.50 – 0.56
M_2 (M_{\odot})	0.14 – 0.20
T_{CS} (K)	90,000 – 100,000
T_2 (K)	$\lesssim 5000$
R_{CS} (R_{\odot})	0.125 – 0.180
R_2 (R_{\odot})	0.3 – 0.4
i ($^{\circ}$)	45 – 50
a (R_{\odot})	1.73 – 1.79

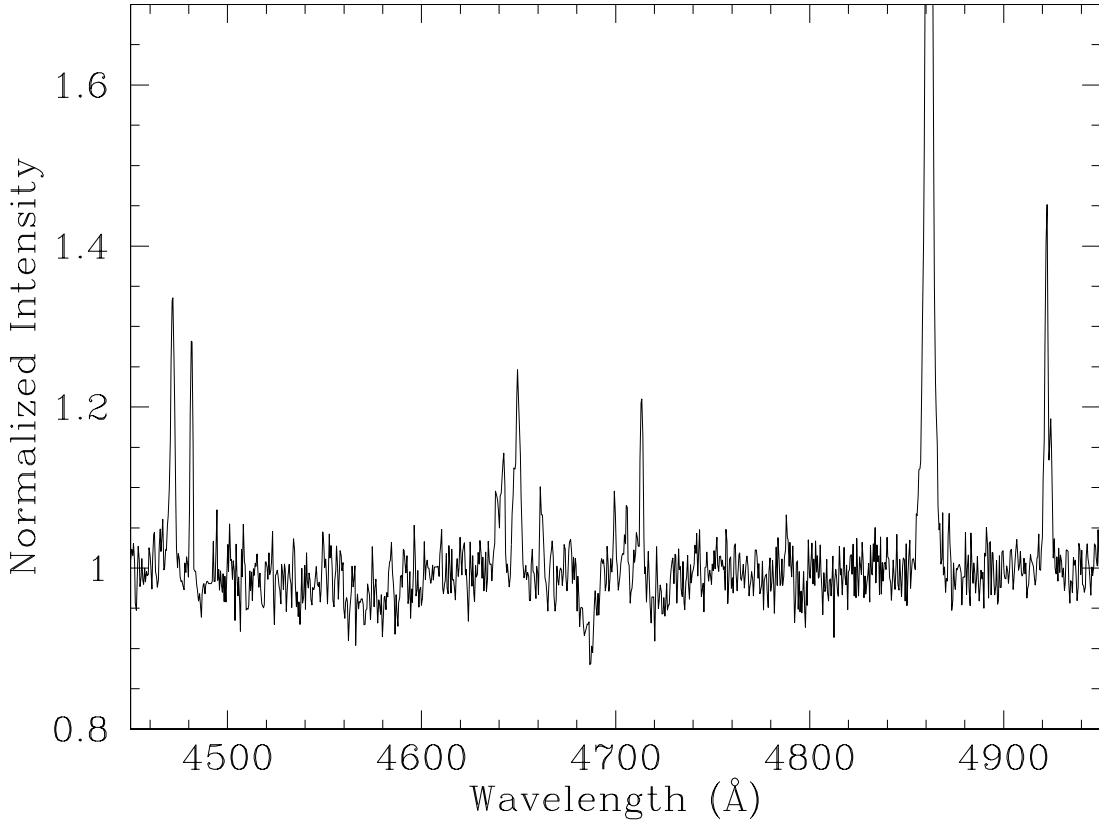


Fig. 11.— A sample spectrum of the CS of ESO 330-9. The C, N, and O complex of emission lines near 4650 Å due to irradiation of a cool companion is evident as are other lines as described in the text. Very faint He II absorption from the hot CS is also present.

Unfortunately, the He II absorption is too broad and noisy to give reliable radial velocity measurements at the low radial velocity amplitudes observed here. A radial velocity curve for the companion is given in Figure 12. The figure shows data points for the emission lines at the photometric period and one-quarter phase shifted from the photometry, demonstrating that they do occur in the companion and are due to irradiation. The dashed and solid lines are example fits for the companion and CS, respectively, from the binary modeling described below.

3.3. Binarity and System Parameters

The low observed radial velocity amplitude of the companion is $15 - 18 \text{ km s}^{-1}$, meaning that either the system is at very low inclination angle, or the mass ratio, $q = M_2/M_{CS}$ is high. Given the short orbital period the secondary star cannot be large. Possible orbital separations for the system are typically less than $2.5 R_\odot$. At inclinations of greater than $i = 25^\circ$, in order for the companion star to fit inside its Roche lobe the mass ratio must be greater than about 3 and results in a CS with a mass below about $0.15 M_\odot$, which is unlikely, especially given that the CS is ionizing the nebula and is hot enough to produce the observed He II absorption line. To have a CS consistent with evolutionary models and hot enough to ionize the nebula, along with a companion that fits inside its Roche lobe, we find a maximum inclination of $i \approx 15^\circ$. That requirement also leads to a companion mass less than $\approx 1 M_\odot$.

We keep in mind in this process that the *observed* radial velocity amplitude is the minimum value for the true orbital velocity of the companion. This is because the curve is determined using the irradiation emission lines which are produced on the hot hemisphere of the star. Thus the center of light is closer to the system center of mass, giving lower velocities than for the center of the star. The values given above consider the possibility that the companion fills a large portion of its Roche lobe over the various mass ratios and inclinations.

Including the light curves allows us to further constrain the inclination as well as the temperatures and radii of the two stars. We find that CS temperatures greater than about 80,000 K cannot reproduce the observed light curves. Given that our solution to the binary modeling for the CS of HaTr 7 required changing the limb-darkening parameters, we consider the effect of repeating that for this system. However, our observation of low ionization in the irradiation spectrum (the strong He I and lack of He II) and the low-excitation nebular spectrum from Frew (2008) are both consistent with a relatively cool companion, so we maintain the internally calculated limb darkening values from the Wilson-Devinney code

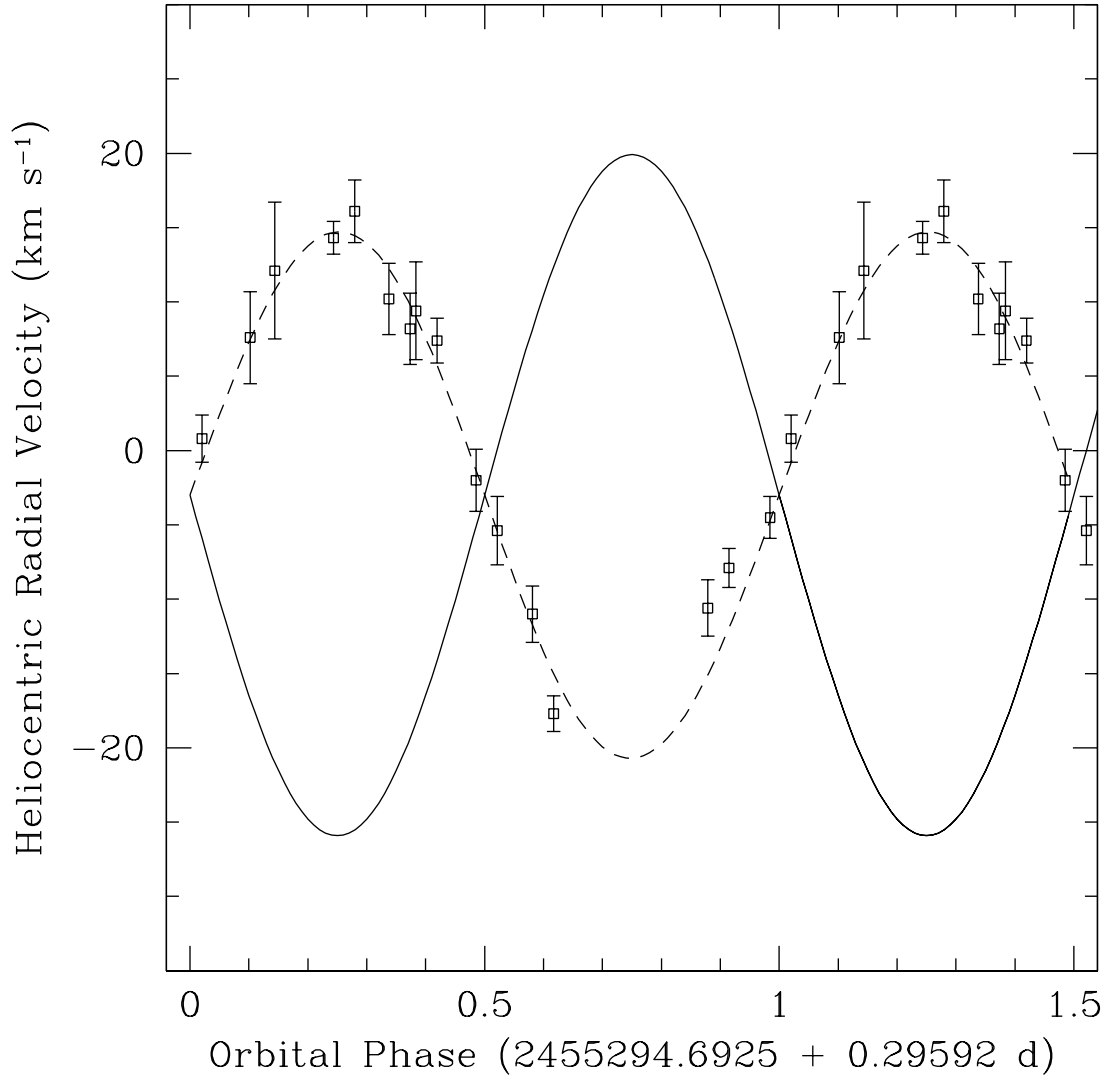


Fig. 12.— The radial velocity curve for the CS of ESO 330-9. Data points are for the irradiation lines described in the text. The dashed line is the radial velocity curve for the irradiated companion, the solid line is the expected curve for the CS, based on one of our best-fit parameter sets from binary modeling.

until we determine if consistent model solutions are possible.

The solutions we find with T_{CS} near 80,000 K result in companion stars with radii significantly smaller than expected for a main sequence star of the equivalent temperature. And while companions in these systems are often higher temperature than their MS counterparts, they are also typically larger. Thus we are left with lower temperatures for the CS. We find that CS temperatures around 55,000 – 65,000 K give values for temperature and radius for both the CS and companion that are consistent with real stars. However, the luminosity we find for the CS is very much smaller than what would be expected for a CO-core post-AGB star. Comparing our model temperature and luminosity values to the evolution curves of Driebe et al. (1998) and Hall et al. (2013), the CS in our models is consistent with a He-core post-RGB object with masses around 0.38–0.45 M_{\odot} (see Figure 5). Assigning the CS a mass of 0.40 M_{\odot} and solving for the system values for our best-fit binary models gives a companion mass of $M_2 \approx 0.36 M_{\odot}$ with $R_2 \approx 0.42 R_{\odot}$ and $T_2 \approx 3700$ K. All of these values are consistent with an over-luminous MS companion in the system. We show our best-fit range of binary system values in Table 2.

While the models in Table 2 provide parameters consistent with physically realistic stars, the evolutionary times present a problem. For a post-RGB star with T and $\log L/L_{\odot}$ of our model, the evolutionary time from Driebe et al. (1998) is 102,000 years and about 98,000 years from Hall et al. (2013), significantly longer than the expected lifetime for a PN. However, the age estimate we calculated above (§3.1) is also long for a PN. But as we discuss below however, our binary model suggests a distance closer than that of Frew et al. (2016), which would give a correspondingly shorter age of around 45,000 years, roughly half that of the evolutionary age we find for the CS. It is possible that the CE evolution for this type of system could be accelerated beyond that in the models, but there is no specific evidence for such an acceleration for ESO 330-9. Hall et al. (2013) describe a possible situation in which a post-RGB CS can end the CE phase in non-thermal equilibrium, resulting in a faster evolution of the star. It is also possible that the interaction of the nebula with the surrounding ISM has delayed the PN evolution by constraining the expanding envelope spatially and/or by collisional reheating. See section §4 below for further discussion of this topic.

In our discussion to date, we have assumed that ESO 330-9 is a bona fide PN, possibly re-brightened as a result of an ISM interaction (see Wareing 2010). Parker et al. (2016) class it as a likely PN, but, it is possible that ESO 330-9 might be a mimic as it has an appearance and ionization structure similar to K 2-2 (De Marco et al. 2013). Spatially-resolved, high-resolution spectroscopy of the nebula will allow for the determination of its nature, and if a true PN, provide details of the nebular morphology, kinematics, and expansion age.

Using the system brightness values from our model with the measured visual magnitudes, we can calculate a distance to the PN based on our binary modelling, d_{model} . Given the uncertainty in the V magnitudes and in $E(B - V)$, we use the I and near-UV magnitudes along with the binary model and $R = 3.1$ to determine a new $E(B - V)$ value. A value of $E(B - V) = 0.40$ results in a match between the observed magnitudes and the model results if the DENIS magnitude was obtained at minimum light. If the DENIS data gives the maximum light magnitude, we find $E(B - V) = 0.37$. For the near-UV reddening correction we use the UV extinction relation described by Valencic et al. (2004). The resulting distance using the absolute magnitude from our example model (see Table 2 and de-reddened apparent magnitude in the I band) is about 0.73–0.91 kpc. The uncertainty in distance increases for our full range of models from Table 2 for which we arrive at $0.7 \lesssim d_{model} \lesssim 1.0$ kpc.

Recall that the distance from Frew et al. (2016) is 1.73 ± 0.51 kpc. Our range is not in good agreement with their value. It is possible that the discrepancy is due to the apparent interaction of the PN with the local ISM. With the $S_{H\alpha} - r$ relation used by Frew et al. (2016), an ISM interaction will usually mean an artificial brightening of the PN, leading to an *underestimated* distance—resulting in a greater discrepancy with our distance. However, the clear asymmetry of the PN (see Figure 7) likely also means that the radius is underestimated, bringing the distance back to smaller values. Another related factor is seen in Figure 5 of Frew et al. (2016) where they show some dispersion in the $S_{H\alpha} - r$ relation due to the mass of the CS, where lower mass CSs fall lower in the plot. Continuing that relation for the likely mass we find for the CS of ESO 330-9 would lead to a much smaller distance for the same surface brightness.

Without understanding better the ISM interaction in the PN we cannot predict whether our distance and that of Frew et al. (2016) could be brought into agreement. However, the dispersion in the relation due to mass does correct in the right direction to bring the two toward better agreement, so we tentatively suggest that between that consideration and the uncertainties involved in the two distance determinations, our different values of distance do not present an insurmountable problem for the physical parameters we find from our binary modeling.

4. Post-RGB evolution and PNe

Observational evidence for multiple evolutionary pathways to planetary nebula formation is suggestive but not yet unequivocal (Frew & Parker 2010; Frew et al. 2014; Reindl et al. 2014). No reliable candidates for post-RGB planetary nebulae were identified by Hall et al. (2013), while a candidate for a post-EHB nebula, PHL 932, was shown by Frew & Parker

(2010) to be ionized interstellar matter. On the other hand, Geier et al. (2011) propose that the similar nebula EGB 5 might be the result of a CE ejection. Since then, Hillwig et al. (2016a) identified HaTr 4 and Hf 2-2 as candidate close-binary initiated post-RGB nebulae. Also, Jones et al. (2016) have identified Abell 46 as another possible post-RGB PN. The hot CS in Abell 46, V477 Lyr, has a measured mass of $0.508 \pm 0.046 M_{\odot}$ (Afşar & Ibañoğlu 2008), which is borderline between post-AGB and post-RGB evolution. Their low temperature of 49500 ± 4500 K is also consistent with a post-RGB object. However, Shimansky et al. (2008) give $T = 83000 \pm 5000$ K, though their reported mass value for the CS of $0.556 \pm 0.096 M_{\odot}$ could still allow for a post-RGB CS. However, Jones et al. (2016) also note that post-RGB evolution may be mechanism through which high and extreme abundance discrepancy factors could be explained, with Abell 46 having a high ADF value.

In Table 3, we summarize the five objects currently considered as possible post-RGB planetary nebulae, including the CS of ESO 330-9, along with three hot stars with similar properties, but which are currently thought to be ionizing regions of ambient ISM (Frew et al. 2010, 2014; De Marco et al. 2013) though Ransom et al. (2010, 2015) offer a contrary opinion.

Some other PNe which may host low-luminosity CSs as inferred from the distances and flux data in Frew et al. (2016) and Parker et al. (2016) are Hen 2-105 (Weidmann & Gamen 2011), Sp 3 (Gauba et al. 2001), NGC 6026 (Hillwig et al. 2010; Danehkar et al. 2013), K 1-2 (Exter et al. 2003), RWT 152 (Aller et al. 2016), SkAc 1 (Douchin et al. 2015), and M 3-57 (= HaWe 11; Hartl & Weinberger 1987). Further work is needed to place them in the HR diagram, before they can be considered as candidate post-RGB PNe.

Recent models of CE interactions (De Marco & Soker 2011; Nie et al. 2012; Madappatt, De Marco, & V 2016) predict that as many post-RGB as post-CE close binary stars may be produced. Those studies typically do not include post-RGB systems as PNe since typical evolutionary times (Driebe et al. 1998; Hall et al. 2013) are much longer than predicted PN lifetimes. However, Hall et al. (2013) describe possible cases in which post-RGB systems may produce a visible PN, which they suggest can occur for CS masses greater than about $0.26 M_{\odot}$. It is not clear from their work what fraction of CSs greater than this mass may form a visible PN, but most populations synthesis and CE evolution models predict that a majority of post-RGB objects will have masses in this range. There is a possibility then that a significant fraction of post-RGB objects may produce a visible PN, and that this fraction may even approach the fraction of PNe with post-AGB close binaries. The statistics to date for CSPNe (e.g. Hillwig 2014) show far fewer post-RGB objects currently known than post-AGB close binaries. However, the distances to many close-binary PNe are not very reliable, so it is possible that some systems currently thought to be post-AGB objects may result instead from post-

RGB evolution. Furthermore, Kamath et al. (2016) has recently found a population of dusty post-RGB stars in the LMC that may have formed as a result of binary interaction. Whether these objects are the precursors of post-RGB PNe remains to be determined. Eventually accurate distances from the GAIA survey (Gaia Collaboration et al. 2016) will allow the luminosities of each system to be reliably measured, allowing for their exact evolutionary origins to be determined, and allowing for a comparison with population-synthesis models. Obtaining orbit-resolved spectra for more of these close binary CSPNe will also allow more detailed binary modeling which can produce CS masses, providing a further test of evolutionary channels.

5. Summary

The CSs of both HaTr 7 and ESO 330-9 show photometric variability due to an irradiated cool companion. The variability period for each system is equal to the orbital period determined from radial velocity curves. For HaTr 7, the binary CS is a double-lined spectroscopic binary showing emission lines from the irradiated hemisphere of the companion and both hydrogen Balmer and He II absorption lines. For the CS of ESO 330-9 we have a single-lined radial velocity curve based on emission lines from the companion.

We have determined orbital periods along with producing limits on the physical parameters for each system using binary modeling. In the case of HaTr 7 the double-lined radial velocities along with modeling of the spectral lines provided much tighter constraints on the system parameters. For that system, our CS parameters from spectral modeling and binary modeling are in agreement with one another, though we find that in order to properly reproduce the light curves we need to modify the limb darkening coefficients for the companion star.

The CS of ESO 330-9 however, is only consistent with theoretical evolutionary tracks if the star is a He-core, likely post-RGB object. The temperature and luminosity of the CS required to fit the light curves corresponds to a well-evolved object with mass $\approx 0.4 M_{\odot}$ that is significantly older than would be expected for a CSPN. Though it is possible that the evolution of the CS was accelerated due to the binary interaction and possible non-thermal equilibrium processes. The possibility of a post-RGB close-binary CSPN would be an interesting test of existing models of PN evolution as well as the formation of close binaries through CE evolution. More detailed studies of the nebular expansion rate, ionization, and composition would help to clarify the picture.

Using our parameter ranges we calculate a distance to each PN. For HaTr 7 the distance

Table 2. ESO 330-9 Best-Fit Binary System Parameters

Parameter	Range	Example ^a
T_{CS} (kK)	55–65	60
M_{CS} (M_{\odot})	0.38–0.45	0.40
T_2 (K)	$\lesssim 4500$	3700
R_{CS}	0.03–0.07	0.040
M_2 (M_{\odot})	0.3–0.5	0.36
R_2	0.35–0.50	0.42
a (R_{\odot})	1.6 – 1.8	1.71
q	0.8 – 1.2	0.90
i ($^{\circ}$)	7 – 13	9.5

^aSee text for details

Table 3: Candidate post-RGB PNe

Name	T_{eff}	$\log g$	Status*	References	Notes
HaTr 4	60000 ± 10000	...	T	HB16	...
Hf 2-2	79000 ± 8000	...	T	HB16	High ADF
Abell 46	49500 ± 4500	5.67 ± 0.05	T	PB94, AI08	High ADF
ESO 330-9	60000 ± 5000	...	L	This work	...
HaWe 13	68100 ± 9400	6.38 ± 0.31	P	HW87, N99, FP16	subluminous PN?
K 2-2	67000 ± 11000	6.09 ± 0.24	N	N99, DM13	mimic
Sh 2-174	69100 ± 3000	6.70 ± 0.18	N	N99, FP10	mimic
DHW 5	76500 ± 5800	6.65 ± 0.19	N	N99, FP10	mimic

References: AI08 – Afşar & Ibanoglu (2008); DM13 – De Marco et al. (2013); FP10 – Frew & Parker (2010); FP16 – (Frew et al. 2016); HB16 – Hillwig et al. (2016a); HW87 – Hartl & Weinberger (1987); N99 – Napiwotzki (1999); PB94 – Pollacco & Bell (1994); * Parker et al. (2016).

range is consistent with distances found previously, though for ESO 330-9 the agreement is marginal, with our results showing a system that is significantly closer.

ESO 330-9 is a diffuse PN that clearly seems to be interacting with the surrounding ISM. As such it does not have any clear large-scale structure or symmetries that would allow determination of an inclination that could be matched to the inclination of the binary system from our modeling. However, HaTr 7 shows a symmetric structure that, though it is faint, could potentially be modeled to find an inclination. This could then be compared to our binary system inclination and added to the collection of systems for which both are known (see Hillwig et al. 2016b).

Apart from comparing inclinations, we have added two more systems to the growing number of close binary CSPNe. As the sample grows we can make increasingly statistically significant studies of close binary CSPNe. Those studies will be able to tell us more about CE evolution, PN formation and ejection, and potentially the formation of cataclysmic variables and type-Ia supernova progenitors.

The authors would like to thank David Jones for helpful comments on the text. This material is based upon work supported by the National Science Foundation under Grant No. AST-1109683. Any opinions, findings, and conclusions or recommendations expressed in this material are those of the author(s) and do not necessarily reflect the views of the National Science Foundation. Based on observations obtained with the SARA Observatory 0.6 m telescope at Cerro Tololo, which is operated by the Southeastern Association for Research in Astronomy (saraobservatory.org). Based on observations (GS-2012A-Q-85 and GS-2015A-Q-97) obtained at the Gemini Observatory, processed using the Gemini IRAF package, which is operated by the Association of Universities for Research in Astronomy, Inc., under a cooperative agreement with the NSF on behalf of the Gemini partnership: the National Science Foundation (United States), the National Research Council (Canada), CONICYT (Chile), Ministerio de Ciencia, Tecnología e Innovación Productiva (Argentina), and Ministério da Ciência, Tecnologia e Inovação (Brazil). The CSS survey is funded by the National Aeronautics and Space Administration under Grant No. NNG05GF22G issued through the Science Mission Directorate Near-Earth Objects Observations Program. The CRTS survey is supported by the U.S. National Science Foundation under grants AST-0909182 and AST-1313422.

Facility: Gemini: South, SOAR, SARA:CTIO

REFERENCES

- Afşar, M., & Ibañoğlu, C. 2008, *MNRAS*, 391, 802
- Aller, A., Miranda, L. F., Olguín, L., Solano, E., & Ulla, A. 2016, *MNRAS*, 462, 3945
- Basurah, H. M., Ali, A., Dopita, M. A., et al. 2016, *MNRAS*, 458, 2694
- Bloecker, T. 1995, *A&A*, 299, 755
- Boffin, H. M. J., Jones, D., Beletsky, Y., et al. 2012, *The Messenger*, 148, 25
- Bond, H. E., & Grauer, A. D. 1987, *IAU Colloq. 95: Second Conference on Faint Blue Stars*, 221
- Chu, Y.-H., Gruendl, R. A., Guerrero, M. A., et al. 2009, *AJ*, 138, 691
- Claret, A. 2000, *A&A*, 363, 1081
- Corradi, R. L. M., García-Rojas, J., Jones, D., & Rodríguez-Gil, P. 2015, *ApJ*, 803, 99
- Danehkar, A., Frew, D. J., De Marco, O., & Parker, Q. A. 2013, *Binary Paths to Type Ia Supernovae Explosions*, 281, 221
- De Marco, O. 2009, *PASP*, 121, 316
- De Marco, O., Hillwig, T., & Smith, A.J. 2008, *AJ*, 136, 323 (Paper I)
- De Marco, O., & Soker, N. 2011, *PASP*, 123, 402
- De Marco, O., Passy, J.-C., Frew, D. J., Moe, M., & Jacoby, G. H. 2013, *MNRAS*, 428, 2118
- Douchin, D., De Marco, O., Frew, D. J., et al. 2015, *MNRAS*, 448, 3132
- Drake, A. J., Djorgovski, S. G., Mahabal, A., et al. 2009, *ApJ*, 696, 870
- Driebe, T., Schoenberner, D., Bloecker, T., & Herwig, F. 1998, *A&A*, 339, 123
- Exter, K. M., Pollacco, D. L., & Bell, S. A. 2003, *MNRAS*, 341, 1349
- Frew, D., 2008, PhD dissertation, Macquarie University, Sydney, Australia
- Frew, D. J., & Parker, Q. A. 2007, *Asymmetrical Planetary Nebulae IV*, 68
- Frew, D. J., Madsen, G. J., O’Toole, S. J., & Parker, Q. A. 2010, *PASA*, 27, 203
- Frew, D. J., & Parker, Q. A. 2010, *PASA*, 27, 129

- Frew, D. J., Bojičić, I. S., Parker, Q. A., et al. 2014, *MNRAS*, 440, 1345
- Frew, D. J., Parker, Q. A., & Bojičić, I. S. 2016, *MNRAS*, 455, 1459
- Gaia Collaboration, Brown, A. G. A., Vallenari, A., et al. 2016, arXiv:1609.04172
- Gauba, G., Parthasarathy, M., Nakada, Y., & Fujii, T. 2001, *A&A*, 373, 572
- Geier, S., Napiwotzki, R., Heber, U., & Nelemans, G. 2011, *A&A*, 528, L16
- Girard, T. M., van Altena, W. F., Zacharias, N., et al. 2011, *AJ*, 142, 15
- Grothues, H.-G., & Kohoutek, L. 1993, *Astronomische Nachrichten*, 314, 297
- Hajduk, M., Zijlstra, A. A., & Gesicki, K. 2008, *A&A*, 490, L7
- Hall, P. D., Tout, C. A., Izzard, R. G., & Keller, D. 2013, *MNRAS*, 435, 2048
- Hartl, H., & Tritton, S. B. 1985, *A&A*, 145, 41
- Hartl, H., & Weinberger, R. 1987, *A&AS*, 69, 519
- Henden, A. A., Templeton, M., Terrell, D., et al. 2016, *VizieR Online Data Catalog*, 2336,
- Hillwig, T. C., Bond, H. E., Afşar, M., & De Marco, O. 2010, *AJ*, 140, 319
- Hillwig, T. C. 2011, *Asymmetric Planetary Nebulae 5 Conference*, Ed. A. A. Zijlstra, F. Lykou, I. McDonald, and E. Lagadec, 275.
- Hillwig, T. 2014, *Asymmetrical Planetary Nebulae VI Conference*, Ed. C. Morisset, G. Delgado-Inglada and S. Torres-Peimbert, 38
- Hillwig, T. C., Frew, D. J., Louie, M., et al. 2015, *AJ*, 150, 30
- Hillwig, T. C., Bond, H. E., Frew, D. J., Schaub, S. C., & Bodman, E. H. L. 2016, *AJ*, 152, 34
- Hillwig, T. C., Jones, D., De Marco, O., Bond, H. E., Margheim, S., & Frew, D. J. 2016, *ApJ*, accepted (arXiv:1609.02185)
- Hirsch, H. A. 2009, Ph.D. Thesis, University Erlangen-Nürnberg
- Huckvale, L., Prouse, B., Jones, D., Lloyd, M., Pollacco, D., López, J. A., O’Brien, T. J., Sabin, L., & Vaytet, N. M. H. 2013, *MNRAS*, 434, 1505

- Iaconi, R., Reichardt, T., Staff, J., De Marco, O., Passy, J.-C., Price, D., & Wurster, J. 2016, arXiv:1603.01953
- Jones, D., Wesson, R., García-Rojas, J., Corradi, R. L. M., & Boffin, H. M. J. 2016, MNRAS, 455, 3263
- Kamath, D., Wood, P. R., Van Winckel, H., & Nie, J. D. 2016, A&A, 586, L5
- Lauberts, A. 1982, Garching: European Southern Observatory (ESO), 1982,
- Madappatt, N., De Marco, O., & Villaver, E. 2016, MNRAS, 463, 1040
- Magakian, T. Y. 2003, A&A, 399, 141
- Miller Bertolami, M. M. 2016, A&A, 588, A25
- Miszalski, B., Acker, A., Parker, Q.A., & Moffat, A.F.J. 2009b, A&A, 505, 249
- Miszalski, B., Jones, D., Rodríguez-Gil, P., et al. 2011, A&A, 531, A158
- Nandez, J. L. A., Ivanova, N., & Lombardi, J. C. 2015, MNRAS, 450, L39
- Nandez, J. L. A., & Ivanova, N. 2016, MNRAS, 460, 3992
- Napiwotzki, R. 1999, A&A, 350, 101
- Nie, J. D., Wood, P. R., & Nicholls, C. P. 2012, MNRAS, 423, 2764
- Ohlmann, S. T., Röpke, F. K., Pakmor, R., & Springel, V. 2016, ApJ, 816, L9
- Parker, Q. A., Acker, A., Frew, D. J., et al. 2006, MNRAS, 373, 79
- Parker, Q. A., Bojčić, I. S., & Frew, D. J. 2016, Journal of Physics Conference Series, 728, 032008
- Passy, J.-C., De Marco, O., Fryer, C. L., et al. 2012, ApJ, 744, 52
- Pollacco, D. L., & Bell, S. A. 1994, MNRAS, 267, 452
- Ransom, R. R., Kothes, R., Wolleben, M., & Landecker, T. L. 2010, ApJ, 724, 946
- Ransom, R. R., Kothes, R., Geisbuesch, J., Reich, W., & Landecker, T. L. 2015, ApJ, 799, 198
- Rauch, T., & Deetjen, J. L. 2003, Stellar Atmosphere Modeling, 288, 103

- Reindl, N., Rauch, T., Werner, K., Kruk, J. W., & Todt, H. 2014, *A&A*, 566, A116
- Reindl, N., Geier, S., Kupfer, T., et al. 2016, *A&A*, 587, A101
- Ricker, P. M., & Taam, R. E. 2012, *ApJ*, 746, 74
- Santander-García, M., Rodríguez-Gil, P., Corradi, R. L. M., et al. 2015, *Nature*, 519, 63
- Saurer, W., Werner, K., & Weinberger, R. 1997, *A&A*, 328, 598
- Schlaffly, E. F., & Finkbeiner, D. P. 2011, *ApJ*, 737, 103
- Schönberner, D. 1983, *ApJ*, 272, 708
- Schöning, T., & Butler, K. 1989, *A&AS*, 78, 51
- Shimansky, V. V., Pozdnyakova, S. A., Borisov, N. V., et al. 2008, *Astronomy Letters*, 34, 423
- Tremblay, P.-E., & Bergeron, P. 2009, *ApJ*, 696, 1755
- Valencic, L. A., Clayton, G. C., & Gordon, K. D. 2004, *ApJ*, 616, 912
- Wareing, C. J. 2010, *PASA*, 27, 220
- Weidmann, W. A., & Gamen, R. 2011, *A&A*, 531, A172
- Weidmann, W. A., Méndez, R. H., & Gamen, R. 2015, *A&A*, 579, A86
- Werner, K., Deetjen, J. L., Dreizler, S., et al. 2003, *Stellar Atmosphere Modeling*, 288, 31
- Wilson, R.E. 1990, *ApJ*, 356, 613
- Wilson, R.E., & Devinney, E. J. 1971, *ApJ*, 166, 605
- Zacharias, N., Finch, C. T., Girard, T. M., et al. 2012, *VizieR Online Data Catalog*, 1322,
- Zijlstra, A. A. 2007, *Baltic Astronomy*, 16, 79